

# RotaTR: Detection Transformer for Dense and Rotated Object

Yuke Zhu, Yumeng Ruan, Lei Yang, Sheng Guo  
Mybank Technology

{felix.yk, guosheng.guosheng}@mybank.cn

## Abstract

*Detecting the objects in dense and rotated scenes is a challenging task. Recent works on this topic are mostly based on Faster RCNN or Retinanet. As they are highly dependent on the pre-set dense anchors and the NMS operation, the approach is indirect and suboptimal. The end-to-end DETR-based detectors have achieved great success in horizontal object detection and many other areas like segmentation, tracking, action recognition and etc. However, the DETR-based detectors perform poorly on dense rotated target tasks and perform worse than most modern CNN-based detectors. In this paper, we find the most significant reason for the poor performance is that the original attention can not accurately focus on the oriented targets. Accordingly, we propose Rotated object detection TRansformer (RotaTR) as an extension of DETR to oriented detection. Specifically, we design Rotation Sensitive deformable (RSDeform) attention to enhance the DETR's ability to detect oriented targets. It is used to build the feature alignment module and rotation-sensitive decoder for our model. We test RotaTR on four challenging-oriented benchmarks. It shows a great advantage in detecting dense and oriented objects compared to the original DETR. It also achieves competitive results when compared to the state-of-the-art. The code will be released.*

## 1. Introduction

Oriented object detection is a more general and challenging task than conventional horizontal detection. It has a wide range of applications in scene text detection[16][51], aerial object detection[44][22], faces and retail scenes[32][4].

Nowadays, most state-of-the-art methods[48][9][7][45] on oriented detection are based on Faster RCNN[29] or Retinanet[19]. They highly depend on pre-set dense anchors for box regression and non-maximum suppression (NMS) for duplicate removal. These two hand-crafted modules lead to a tedious and redundant detection process, which is an indirect and sub-optimal solution to the oriented

detection problem. In contrast, the idea of end-to-end object detection has been favored by many researchers in conventional detection. A lot of methods have been proposed to design an end-to-end detector from the perspective of anchor free[13][28][17][35], NMS free[12][8][33][38][34] or the recent transformer[1][42][20] structure. However, in oriented detection, there are few works addressing this issue.

Recently, DETR[1] and its followers[54][42][20] bring new insight into the detection paradigm. The DETR regards object detection as a sequence-to-sequence problem. It uses a set of object queries to probe into the image context and directly generates a set of predictions without the need for NMS. The new paradigm of DETR is general and has been successfully adapted to many other areas like instance segmentation[52][6][5], action recognition[46][21][31], multi-object tracking[41][14][43] etc. So, it is a natural thought that DETR-like structures can also be easily adapted to oriented object detection. Based on the idea, we design a simple oriented detector Deformable-DETR-O based on Deformable DETR[54] (detailed in Sec-3.1) and test it on the common oriented benchmark. However, the results are frustrating. The adapted detector performs even inferior to Retinanet-O, which usually serves as the baseline method for most oriented detection methods (Shown in Table-1). The poor performance is especially significant for densely located targets. The phenomenon can also be supported by some observations from DAB-DETR[20], which reports a lot of failure cases in dense scenes. The recently published O2DETR[24] is the first attempt to design DETR-like oriented detector. It also reports low performance on such occasions. So far, no other work has attempted to explain the poor performance of DETR-like structures for oriented and densely located targets. To this end, we take a closer look at the cross-attention module in the transformer decoder. Specifically, the sampled locations of the deformable cross attention are visualized. The result shows that the sampled locations of the deformable attention (Shown in Figure-4(d)) can hardly be aligned with the target geometry. It suggests that it is difficult for deformable attention to dynamically attend to arbitrarily ori-

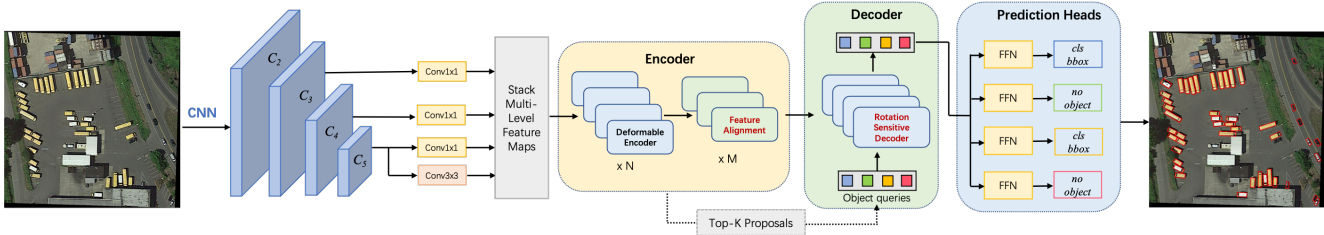


Figure 1: A schematic overview of RotaTR. Note that the RotaTR can be used in the two-stage form and one-stage form. When in two-stage form, the encoder will generate top-k proposals as the initialization for the decoder query.

ented targets.

In this paper, we propose Rotated object detection Transformer (RotaTR) as a solution to extend DETR to oriented object detection. Motivated by the above observation, we design Rotation Sensitive Deformable (RSDeform) attention to enhance the deformable attention with the ability to learn orientations. In RSDeform, the orientation, as well as the bounding box’s geometry, are explicitly exploited to guide the attention sampling. The RSDeform forms the basic building block for the decoder. Besides, we also use it to build a feature alignment module to solve the feature misalignment problem caused by arbitrary orientation. The RSDeform introduces no extra parameters and computation for oriented sampling can be neglected. Besides, we also follow the DAB-DETR[20] to introduce the concept of dynamic anchors to simplify the query design. We also notice that the regression of the rotated bounding box may encounter the problem of ambiguity and in-continuity. The regression issue has been discussed by a large number of researchers[49][27]. Inspired by previous work, we design a simple point set loss to calculate the distance between the predicted and target point set. The point set loss is simple and intuitive and proves effective in our experiments.

In summary, the contributions of this work include: (1) We propose RotaTR as an extension of DETR to oriented detection. It greatly strengthens the DETR’s ability in capturing arbitrary orientations. (2) We design the RSDeformable attention to facilitate orientated attention. It is an individual module and can be applied to other structures. (3) We propose point set loss as a simple oriented regression loss. It proves effective in both RotaTR and other oriented-detectors.

## 2. Related Work

### 2.1. End-to-End Object Detection

End-to-end object detection refers to the detection system that is free of any non-differentiable modules. Early methods towards end-to-end detection are based on CNN detectors. Most of them aim to eliminate the anchors[35][28][26] or nms[12][8] operation.

Recently, DETR[1] proposes a transformer-based end-

to-end detector. Since its publication, it has attracted great attention and a lot of successors[54][42][25][20] have been proposed. Later, some CNN-based methods[33][38][34] also followed a similar idea of DETR to design the NMS-Free detector.

In contrast, for oriented object detection, the efforts toward end-to-end detection are nearly absent. The recent work O2DETR[24] first attempts to introduce the DETR into oriented detection. However, the poor performance of DETR in dense scenes is not solved. The final performance lags far behind most of the SOTA CNN-based methods.

### 2.2. Feature Misalignment in Oriented Detection

In object detection, feature alignment refers to the spatial alignment between image features and anchor boxes. For example, Mask RCNN[10] proposes RoIAlign, which uses bi-linear interpolation to replace max-pooling to avoid the quantization error in RoIPooling[29], thus leading to better alignment between extracted features and anchors. Following work like Guided Anchoring[37], AlignDet[3] also seek to better align features with anchors for accurate feature extraction.

For oriented detection, the introduction of angle dimension makes feature alignment more important. For better feature alignment, R3Det[48] adds Feature Refinement Module to reconstruct the feature map. S2ANet[9] designs Feature Alignment Module and Oriented Detection Module to generate high-quality anchors and aligned features. Oriented RCNN[45] uses Rotated RoIAlign to extract rotation-invariant features from oriented proposals generated from oriented RPN.

In this work, we also find that the core reason for the poor performance of DETR in oriented detection is the lack of alignment ability. The proposed RotaTR uses specially designed RSDeform attention to solve this problem.

## 3. Method

### 3.1. Adapting DETR for Rotated Object

The first step to adapt DETR to rotated detection is to add an extra channel for the angle regression. Since two quadrants are enough to represent any rotated box, we restrict

the angle to a certain range, e.g.  $[-\pi/2, \pi/2]$ , to remove its periodicity. Given a decoder embedding  $x$ , the predicted rotated box is computed as:

$$(x, y, w, h, \hat{\theta}) = \sigma(\text{FFN}(x)) \quad (1)$$

where  $\hat{\theta}$  is the intermediate output for the angle without unit.  $\sigma$  is the sigmoid operation. The final angle is got by  $\theta = \hat{\theta}A - A/2$  where  $A$  is the pre-defined angle range.

As the original DETR converges slowly and performs poorly compared with its successors, we choose the Deformable-DETR as our baseline method. Similar to Deformable-DETR, the regression target is defined as the increment with respect to the previous prediction  $\mathbf{p} = (p_x, p_y, p_w, p_h, p_\theta)$ . Given the regression  $(\delta\hat{x}, \delta\hat{y}, \hat{w}, \hat{h}, \hat{\theta}) = \text{FFN}(x)$ , the final predicted bounding box  $(x, y, w, h, \theta)$  is computed as

$$\begin{aligned} (x, y) &= (\sigma(\delta\hat{x} + \sigma^{-1}(p_x)), \sigma(\delta\hat{y} + \sigma^{-1}(p_y))) \\ (w, h) &= (\sigma(\delta\hat{w} + \sigma^{-1}(p_w)), \sigma(\delta\hat{h} + \sigma^{-1}(p_h))) \\ \theta &= A\sigma(\delta\hat{\theta} + \sigma^{-1}(p_\theta)) - A/2 \end{aligned} \quad (2)$$

where  $\sigma^{-1}$  is the inverse sigmoid function.

The optimization process is kept identical to the Deformable DETR, which uses the combination of Focal loss, L1 loss, and IoU loss as the supervision and utilizes the Hungarian matching algorithm to assign labels. The difference is that we use the Rotated-IoU loss to substitute the horizontal IoU loss. Besides, the L1 loss is applied to 5-D rotated boxes.

### 3.2. Overall Architecture

**Structure Overview.** The structure of RotaTR is shown in Figure-1. Following recent work on improving DETR, we design RotaTR based on two main ideas. Specifically, we use dynamic anchor[20] to simplify the query design and multi-scale deformable attention[54] for faster convergence.

The encoder shares a similar structure with Deformable-DETR. The only difference is that we replace the last  $M$  layers with feature alignment layers. We will introduce it in Sec-3.4. The decoder is a stack of rotation-sensitive decoder layers. Each layer is composed of a regular multi-head self-attention, a rotation-sensitive deformable (RSDeform) cross-attention, and a feed-forward layer.

One point worth noting is that RotaTR also has a two-stage form like Deformable-DETR. In the two-stage form, the decoding queries are initialized by the top-k selected proposals generated by the encoder output. We refer the readers to [54] for details.

The key component of both the alignment layer and RSDeform Attention layer is the RSDeform attention, which learns to explicitly modulate the sampling locations based

on the given reference anchors and aggregate the sampled features. It is detailed in Sec-3.3.

**Query Design.** We follow the idea of DAB-DETR[20] to design the dynamic-oriented anchor and use it to form our query. Given a dynamic anchor box  $A_q = (x_q, y_q, w_q, h_q, \theta_q)$ , its positional query  $p_q$  is generated by:

$$p_q = \text{MLP}(\text{PE}(A_q)) \quad (3)$$

where PE means the operation to generate sinusoidal embeddings from float numbers. It encodes both the coordinates of anchor boxes and the angular information:

$$\text{PE}(A_q) = \text{CAT}(\text{Pe}(x_q), \text{Pe}(y_q), \text{Pe}(w_q), \text{Pe}(h_q), \sin(\theta), \cos(\theta)) \quad (4)$$

where CAT means the tensor concatenation operation and Pe is the sinusoidal generation function identical to the that in DETR[1].

In self-attention, the query, key, and value embeddings are defined by:

$$\begin{aligned} \text{Query, Key} &:= c_q + p_q \\ \text{Value} &:= c_q \end{aligned} \quad (5)$$

where  $c_q$  represents the content embedding (decoder embedding). In cross attention, it is similar to that in Deformable DETR except that we change the reference point to a dynamic anchor  $A_q$  and change deformable attention to RSDeform attention.

### 3.3. Rotation Sensitive Deformable Attention

For standard multi-scale deformable attention, it calculates the sampled locations for each reference anchor and then samples over the input multi-level features and sums the sampled features using learned attention weight. Given with a single-level feature map  $x \in \mathbb{R}^{C \times H \times W}$ , query embedding  $z_q$ , and its reference anchor  $A_q = (\mathbf{p}_q, w_q, h_q, \theta_q)$  with  $\mathbf{p}_q = (x_q, y_q)$ , the deformable attention in a single head is calculated by

$$\text{Deform}(z_q, A_q, x) = \sum_{k=1}^K W_{qk} W' x(\mathbf{p}_q + \Delta\mathbf{p}_{qk}) \quad (6)$$

where  $k$  indexes the sampled keys and  $K$  is the total number of keys.  $W'$  is the projection weight for input image features.  $W_q \in \mathbb{R}^{1 \times K}$  is the attention weight calculated by  $W_q = \text{MLP}(z_q)$ , and  $W_{qk}$  is its  $k$ -th component.  $\Delta\mathbf{p}_q$  is the sampling offsets obtained by  $\Delta\mathbf{p}_q = \text{MLP}(z_q)$ .

RSDeform attention is designed on the basis of two considerations. Firstly, the learned offsets  $\Delta\mathbf{p}_q$  in the original deformable attention are forced to implicitly adapt to the angular variation. While experimentally, we find the adaptability of offsets to orientation is weak. Thus, for each reference anchor  $A_q$ , the modulated offset  $\tilde{\mathbf{p}}_q$  is explicitly calculated by

$$\Delta\tilde{\mathbf{p}}_q = \Delta\mathbf{p}_q \cdot R^T(\theta) \quad (7)$$

where  $R(\theta) = (\cos \theta, -\sin \theta; \sin \theta, \cos \theta)^T$  is the rotation matrix. Secondly, the learned offsets  $\Delta \mathbf{p}_q$  in the original deformable attention are not imposed by any restriction. The observed sampling locations are usually out of the boundary of the target object. The negative effect of inaccurate sampling is especially serious for densely located objects. To fix this problem, the learned offsets are further restricted by the boundary of the reference anchor. The modulated offset is calculated by

$$\Delta \tilde{\mathbf{p}}_q = \alpha \cdot (w, h) \cdot (\sigma(\Delta \mathbf{p}_q) - 1/2) \cdot R^T(\theta) \quad (8)$$

where  $\alpha$  is the hyper-parameter controlling the offset range relative to the reference anchor. By default, the  $\alpha$  is set to 1. Based on the modulated offset, the rotation-sensitive deformable attention is calculated as

$$\text{RSDeform}(z_q, A_q, x) = \sum_{k=1}^K W_{qk} W' x(\mathbf{p}_q + \Delta \tilde{\mathbf{p}}_{qk}) \quad (9)$$

In this way, we can transform the sampling locations to explicitly adapt to arbitrary orientations based on corresponding reference anchors.

The Rotation Sensitive Deformable Attention serves as the basic building block for RotaTR. It is mainly used in two modules. One is the feature alignment module, the other is the decoder layer. The following two parts detail the specific application.

**Comparison with Related Operations** We compare the RSDeform Attention with two most related operators that are commonly used to relieve the feature misalignment problem caused by arbitrary orientation. For clarity, we present the schematic plot in Figure-2. The first related operator is the original form of deformable attention. It learns an offset field to generate the sampling locations. During training, the offset field is adaptive to fit the target object. The second one is the align convolution proposed in S2ANet[9]. Align convolution is built upon the standard convolution and explicitly calculates the offset generated by the orientation. In contrast, the RSDeform attention absorbs the advantages of these two. On one hand, it explicitly calculates the offset field like align convolution, on the other hand, it keeps the capability of adaptive fitting like deformable attention.

### 3.4. Feature Alignment Module

Feature alignment module can be viewed as part of the encoder network. It has a similar structure to the encoder layer, which takes the encoded multi-level features as input. The difference is that, besides attention layers and feed-forward layers, the feature alignment module has two extra branches: anchor classification branch and anchor regression branch. The classification branch distinguishes each pixel of features into foreground and background and the

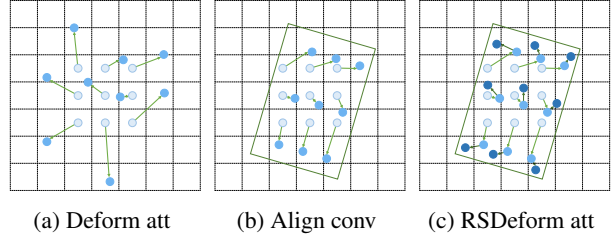


Figure 2: Comparison between different methods for feature alignment. The light blue points denote the initial locations. The arrows represent the calculated offset vectors. (a) is the original deformable attention, it adaptively learns the offset locations. (b) is the alignment convolution proposed in S2ANet[9]. It explicitly computes the offset locations by given orientations. (c) is our proposed RSDeformable attention. It can be viewed as a two-step alignment process. The first step is to get the explicitly computed offset locations. The second step is to adaptively learn the offset locations.

regression branch predicts the extra offset with respect to predefined horizontal anchors for each pixel location. Then the generated rotated anchors are fed into the RSDeform attention as the reference anchors, by which the encoded features are further refined. The whole alignment pipeline is depicted in Figure-3. By default, the anchor classification branch is discarded in the inference phrase to speed up the inference as we only need the rotated anchors to refine the features.

### 3.5. Rotation Sensitive Decoder Layer

The rotation-sensitive decoder layer is composed of three parts: a standard multi-head self-attention layer, a RSDeform cross-attention layer and a feed-forward layer. In the self-attention layer, the query, key and value are defined as Eq-5. In the cross attention layer, we follow DAB-DETR to put a  $\text{MLP}^{(s)}$  to obtain a scalar vector conditional on the content information  $c_q$  and use it to perform element-wise multiplication with the positional encoding:

$$\text{Query} : c_q + p_q \cdot \text{MLP}^{(s)}(c_q) \quad (10)$$

Then, the rotation-sensitive cross attention is calculated by Eq-9.

Following the previous practice, we use the decoder layer to predict the relative reference offset  $(\delta \hat{x}, \delta \hat{y}, \delta \hat{w}, \delta \hat{h}, \delta \hat{\theta})$  and update the reference anchors layer-by-layer.

### 3.6. Optimization Objective

The horizontal detectors usually use L1 loss to regress the bounding boxes. It has two problems. The first is that the value range of coordinates differs far away from the angle range. A weighting factor must be introduced to balance the two regression tasks, while finding the proper weighting factor is not an easy task. The second is that each rotated

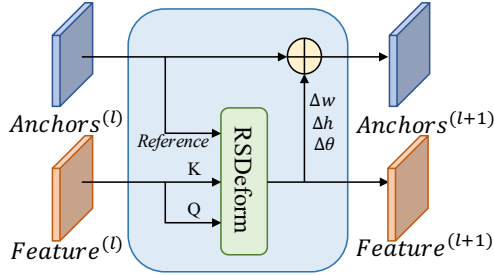


Figure 3: Schematic overview of the feature alignment module of the encoder.

box has two equivalent representations. We can simply exchange the position of width and height and modify the rotation angle correspondingly to get the other representation. This leads to the target ambiguity problem. These two problems have been thoroughly discussed in previous work[49]. To fix this, we propose a simple point set loss for regression. For a predicted box and a target box, we first transform them into two point sets, representing each box’s eight corner points,  $[p_i]$  and  $[q_i]$ . Note that the point set is in the order of either clockwise or counterclockwise. The point set loss is calculated by

$$\mathcal{L}_r = \inf_{\pi} \sum_i \|p_i - q_{\pi(i)}\| \quad (11)$$

where  $\pi(i)$  is an index mapping function from set  $\{0, 1, 2, 3\}$  to itself. The point set loss finds the minimum distance sum between the given two point sets. As the two sets are in order, the number of mapping is limited. Thus the point set loss can be calculated quickly. The final optimization objective is the combination of the focal loss, regression loss and the rotated-IoU loss.

## 4. Experiment

### 4.1. Datasets

We evaluate our method on multiple datasets mainly covering aerial images: DOTA-1.0 and DOTA-1.5[44], ship detection HRSC2016[22], and text detection MSRA-TD500[51].

**DOTA**[44] is one of the largest datasets for multi-class object detection in aerial images with two released versions: DOTA-v1.0 and DOTA-v1.5. **DOTA-v1.0** contains 15 categories, 2,806 images and 188,282 instances. Images’ scales range from  $800 \times 800$  to  $4000 \times 4000$  pixels. It is split into training, validation, and test sets with 1/2, 1/6, and 1/3 ratios, respectively. For the short names in Table-1, they are defined as (abbreviation-full name): BR-Bridge, SV-Small vehicle, LV-Large vehicle, SH-Ship, HA-Harbor, ST-Storage tank, RA-Roundabout, PL-Plane, BD-Baseball diamond. **DOTA-v1.5** shares identical image sets with v1.0. It is released with a new category, Container Crane (CC). In

DOTA-v1.5, more small objects are annotated, making it a much more challenging task compared with v1.0.

For both versions of DOTA datasets, we crop the images into  $1024 \times 1024$  patches with a stride of 120. In the single scale setting, we only adopt random horizontal flipping during training to avoid over-fitting and no other tricks are utilized if not specified. In the multi-scale setting, for fair comparison with other methods, we adopt data augmentation (i.e., random rotation) in the training phase and three scales (0.5, 1.0, 1.5) are used to scale the cropped patches.

**HRSC2016**[22] is another challenging aerial images dataset that contains lots of large aspect ratio ship instances with arbitrary orientation. It is split into training, validation and test set which contains 436 images including 1207 samples, 181 images including 541 samples and 444 images respectively. We use both the training and validation sets for training and test sets for testing.

**MSRA-TD500**[51] is commonly used for oriented scene text detection and spotting. It contains 300 training images and 200 testing images. Extra 400 images from HUST[50] are also included for training.

### 4.2. Implementation Details

We implement the proposed method on MMDetection[2]. In all experiments, we adopt Deformable DETR-O with ResNet-50 backbone (pretrained on ImageNet) as the baseline method. It is the modified version of Deformable DETR to oriented detection. We use multi-scale features from C3 to C5 of ResNet-50. We train the network with AdamW for 50 epochs. In the first 40 epochs, the learning rate is  $1e - 4$  and then  $1e - 5$  for another 10 epochs. The momentum and weight decay are set to 0.9 and 0.001 respectively. We train our method on a single A100 GPU with the batch size of 4. The loss weights for classification, regression and rotated-IoU are set as 2, 5 and 2, respectively. In the inference stage, we follow the same scale setting as training. No post-processing is needed for associating objects.

### 4.3. Comparison Results

**Competitors.** On DOTA dataset and HRSC dataset, we mainly compare our method to several CNN-based methods (i.e., Retinanet-O, RSDet[27], CenterMap[39], R3Det[48], SCRDet[49], S2ANet[9]) and transformer-based methods (i.e., RoI-Transformer[7], O2Transformer[24], Deformable-DETR-O). The Retinanet-O and Deformable-DETR-O are the modified version of the original horizontal Retinanet[19] and Deformable-DETR[54] to oriented detection, respectively. The majority of them are CNN-based methods. Only RoI Transformer and O2DETR are related to transformer. Note that the RoI transformer is not an end-to-end transformer-based detector. It uses transformer only for region proposal generation and should also be

Model	Backbone	Epochs	PL	BD	BR <sup>†</sup>	GTF	SV <sup>†</sup>	LV <sup>†</sup>	SH <sup>†</sup>	TC	BC	ST	SBF	RA	HA <sup>†</sup>	SP	HC	mAP
<i>SingleScale</i>																		
Retinanet-O[19]	R-50-FPN	12	88.67	77.62	41.81	58.17	74.58	71.64	79.11	90.29	82.18	74.32	54.75	60.60	62.57	69.67	60.64	68.43
Retinanet-O*	R-50-FPN	36	88.83	71.62	43.42	63.91	68.22	73.61	86.65	90.82	86.17	83.79	55.82	65.28	65.83	67.66	58.71	71.72
	R-50-FPN	50	88.62	71.21	41.70	64.36	68.08	73.50	86.85	90.27	85.47	83.51	55.31	62.78	65.41	68.45	58.20	71.12
RSDet[27]	R-101-FPN	12	89.80	82.90	48.60	65.20	69.50	70.10	70.20	90.50	85.60	83.40	62.50	63.90	65.60	67.20	68.00	72.20
CenterMap[39]	R-50-FPN	12	88.88	81.24	53.15	60.65	78.62	66.55	78.10	88.83	77.80	83.61	49.36	66.19	72.10	72.36	58.70	71.74
R3Det[48]	R-101-FPN	12	88.76	83.09	50.91	67.27	76.23	80.39	86.72	90.78	84.68	83.24	61.98	61.35	66.91	70.63	53.94	73.79
SCRDet[49]	R-101-FPN	12	89.98	80.65	52.09	68.36	68.36	60.32	72.41	90.85	87.94	86.86	65.02	66.68	66.25	68.24	65.21	72.61
S2ANet[9]	R-50-FPN	12	89.11	82.84	48.37	71.11	78.11	78.39	87.25	90.83	84.90	85.64	60.36	62.60	65.26	69.13	57.94	74.12
S2ANet*	R-50-FPN	36	88.57	83.61	53.21	71.32	77.08	81.69	87.35	90.27	85.91	85.14	52.27	65.09	73.70	66.37	65.80	75.21
	R-50-FPN	50	88.62	81.63	52.91	71.28	79.08	80.22	88.21	90.88	84.24	83.24	59.20	65.12	76.11	71.85	48.03	74.71
RoI-Transformer*[7]	R-50-FPN	36	88.96	81.30	47.89	65.44	80.71	81.62	87.76	90.90	83.90	85.43	58.10	65.06	72.66	72.97	44.68	73.83
Oriented-RCNN*[45]	R-50-FPN	12	89.46	82.12	54.78	70.86	78.93	83.00	88.20	90.90	87.50	84.68	63.97	67.69	74.94	68.84	52.28	75.60
	R-50-FPN	36	88.90	82.91	55.11	71.14	78.99	83.06	88.14	90.90	83.77	85.49	61.76	66.76	76.62	68.85	53.41	75.72
	R-50-FPN	50	88.65	83.42	52.95	73.27	78.88	83.77	87.99	90.88	79.69	85.61	56.67	62.80	77.62	69.65	52.17	74.94
O2Transformer[24]	R-50	50	83.89	75.11	44.04	64.20	78.39	76.78	87.68	90.60	78.58	71.82	53.21	60.35	55.36	61.90	47.89	68.65
FT-O2Transformer	R-50-FPN	50	88.76	81.91	51.20	72.18	77.64	80.47	87.84	90.85	84.56	81.68	61.42	64.61	67.50	64.28	62.15	74.47
Deform-DETR-O[54]	R-50	50	86.91	74.40	47.22	64.31	72.07	76.01	86.66	90.84	78.45	77.57	53.28	60.50	62.41	68.16	50.47	69.95
RotaTR	R-50	50	88.87	82.91	49.67	69.52	79.01	83.58	88.20	90.64	78.99	85.78	54.85	63.44	77.05	73.12	69.06	75.86
<i>Multi - Scale</i>																		
Retinanet-O*[19]	R-50-FPN	36	89.01	84.13	50.92	70.33	71.08	77.21	84.33	90.80	71.63	86.42	61.78	64.25	67.98	69.20	48.04	76.50
RoI-Transformer*[7]	R-101-FPN	36	88.51	86.43	60.74	80.12	77.47	85.10	88.49	90.91	88.67	84.73	70.42	65.78	79.12	80.94	74.65	80.11
O2DETR[24]	R-50	50	86.01	75.92	46.02	66.65	79.70	79.93	89.17	90.44	81.19	76.00	56.91	62.45	64.22	65.80	58.96	72.15
FT-O2DETR	R-50-FPN	50	88.89	83.41	56.72	79.75	79.89	85.45	89.77	90.84	86.15	87.66	69.94	68.97	78.83	78.19	70.38	79.66
RotaTR	R-50	50	88.50	85.91	60.13	78.94	79.80	84.95	89.88	90.94	88.47	86.43	68.58	67.31	81.59	76.88	76.93	79.95
	R-101	50	88.31	85.64	60.44	78.81	79.91	86.22	89.34	90.90	87.71	86.44	71.05	68.67	79.20	82.31	77.56	80.48

Table 1: Comparison to state-of-art on DOTA-v1.0 test set. Results for each class are reported. The best and second best results are colored in red and blue respectively. Classes with <sup>†</sup> superscript denotes the large aspect ratio targets. **SV** and **LV** are in bold. They are most likely to be dense located. The method with \* superscript denotes that the reproduced results. Most of the reproduced results surpass that in the original work.

categorized into CNN-based detectors. On MSRA-TD500 datasets, we choose the commonly used text detectors as the competitors.

**Training Length.** On DOTA dataset, most of the CNN-based detectors adopt the 12-epoch training setting. Actually, increasing the training length to 36 epochs will greatly increase the performance. Continually increasing the training length to 50 won't improve the performance but will overfit. While for our transformer-based methods, 12-epoch training is not enough for convergence. Defiantly, we train 50 epochs for comparison. The training lengths on other datasets are also adjusted according to the actual convergence state.

**Results on DOTA.** The comparison results on DOTA-v1.0 is shown in Table-1. We can see that the transformer-based methods perform much worse than the modern CNN-based methods. For example, the newly proposed O2Transformer gets mAP of 68.65, even inferior to the Retinanet-O (71.72). The Deformable DETR-O gets 69.95. It is also at the same level as O2DETR. By contrast, the proposed RotaTR achieve 75.86% mAP with only ResNet 50 backbone in the single scale, outperforming all the competitors. Note that RotaTR gets very challenging results on SV (small vehicle) and LV (large vehicle). These two are most likely to be densely located.

On DOTA-v1.5 dataset, we report the AP metric under 50% and 75% IoU conditions. The results are shown in Table-2. Specifically, RotaTR gets 70.5% mAP under IoU 50% and 46.2% mAP under IoU 75%, greatly surpassing the baseline method by 4.7% and 10.7%, respectively.

Method	v1.0 train/val			v1.5 train/val		
	AP50	AP75	AP50:95	AP50	AP75	AP50:95
Retinanet-O[19]	66.3	41.7	38.3	67.5	41.3	40.7
R3Det[48]	67.2	38.4	38.4	69.2	44.6	42.6
RoI Transformer[7]	71.3	47.5	44.8	70.2	46.1	43.5
O2DETR[24]	65.3	41.4	39.8	63.8	33.2	35.1
Deformable-DETR-O[54]	67.3	43.7	40.1	65.8	35.5	36.53
RotaTR	<b>72.0</b>	<b>49.0</b>	<b>45.1</b>	<b>70.5</b>	<b>46.2</b>	<b>43.6</b>

Table 2: Comparison on DOTA-v1.0 and v1.5 datasets

**Results on HRSC.** The HRSC2016 dataset contains only one class and the training set has only 617 images. We find that the original training setting (e.g., 50 epochs) is hard for the RotaTR to fully converge. Thus, for this dataset, the training steps are extended to five times of the original. The results are shown in Table-3. It is seen that RotaTR outperforms the baseline method by 2% mAP and achieves comparable performance to the state-of-the-art.

**Results on MSRA-TD500.** The comparison in MSRA-

Methods	Backbone	mAP (07)	mAP (12)
DRN[26]	H-34	-	92.7
R3Det[48]	R-101-FPN	89.26	96.01
S2A-Net[9]	R-101-FPN	90.17	95.01
RRPN[23]	R-101	79.08	85.64
R2CNN[15]	R-101	73.07	79.73
Oriented R-CNN[45]	R-50-FPN	<b>90.4</b>	96.5
RoI Transformer[7]	R-101-FPN	86.2	-
O2Transformer[24]	R-101-FPN	88.2	93.3
Deformable DETR-O[54]	R-50	88.4	94.1
RotaTR	R-50	90.3	<b>96.7</b>

Table 3: Results on HRSC2016

Method	Precision	Recall	H-mean
RRPN[23]	82.0	68.0	74.0
DeepReg[11]	77.0	70.0	74.0
EAST[53]	87.3	67.4	76.1
SegLink[30]	86.0	70.0	77.0
PAN[40]	80.7	77.3	78.9
RRD[18]	87.0	73.0	79.0
MSR[47]	87.4	76.7	81.7
SAE[36]	84.2	<b>81.7</b>	82.9
RotaTR	<b>90.9</b>	77.6	<b>83.8</b>

Table 4: Results on MSRA-TD500

TD500 is shown in Table-4. Similar to HRSC, the training epoch is modified to 250 for fully converge. It is seen that RotaTR also gets very challenging results in scene text detection.

#### 4.4. Ablation Study

By default, the DOTA-v1.0 validation set is used for ablation study.

**The contribution of each part.** We experiment on DOTA-v1.0 to validate the effectiveness of each proposed module. The results are shown in Table-5. It is seen that the naive Deformable DETR gets only 65.4% mAP. The DAB mechanism can slightly increase the performance to 66.0. While adding point set loss can increase the performance to 67.2%. Extra experiments on other detectors shown in Table-6 also show the effectiveness of the point set loss. The largest contribution comes from the RSDeform attention, which boosts the performance by 4% mAP. We also find that simply adding the feature alignment module brings little improvement. The effect of the feature alignment module emerges only when the rotation-sensitive cross-attention module is applied. When all modules are applied, the performance is increased to 72.0%. The effect of the proposed RSDeform can also be proved via the sampled points. As

DAB	RS	FA	PS	AP50
				65.4
✓				66.0 (+0.6)
	✓			69.3 (+3.9)
✓	✓			69.4 (+4.0)
✓		✓		66.2 (+0.8)
✓	✓	✓		70.8 (+5.4)
✓			✓	67.2 (+1.8)
✓	✓	✓	✓	72.0 (+6.6)

Table 5: Ablation study of proposed modules. DOTA-v1.0 is used in this experiment. The results are reported on the DOTA-v1.0 validation set. **DAB** means the dynamic anchor box mechanism. **RS** means the rotation-sensitive cross attention. **FA** means the feature alignment module. **PS** means the point set loss.

Methods	Point Set Loss	AP50	AP75
Retinanet[19]		66.3	41.7
	✓	<b>67.1</b>	<b>42.5</b>
S2A-Net[9]		69.7	42.1
	✓	<b>70.3</b>	<b>42.6</b>
Deformable DETR-O[54]		66.0	41.8
	✓	<b>67.2</b>	<b>43.7</b>
RotaTR		70.8	48.0
	✓	<b>72.0</b>	<b>49.0</b>

Table 6: Effect of Point Set Loss on other detectors. The results are reported on DOTA-v1.0 validation set.

shown in Figure-4, the sampled points from RSDeform can be well aligned with the target boundary. Dropping each property of RSDeform will result in the misalignment.

**Multi-level feature maps.** The multi-level feature pyramid is a common technique to improve performance on small targets. To verify the influence of the selection of feature maps on the model performance, we experiment on several detectors and report the results on Table-7. It is noticed that although adding the  $4\times$  feature map brings considerable performance gain for Retinanet-O (+0.8% mAP), O2DETR (+2.5% mAP) and Deformable-DETR-O (+1.4% mAP), it has little effect for RotaTR. We argue that the performance gain mainly comes from small objects, which are more likely to be suppressed by the feature misalignment problem caused by arbitrary orientation. To figure it out, we re-evaluate Deformable-DETR-O and RotaTR on objects smaller than  $16 \times 16$ . For the former, the APs with C2 and without are 30.7 and 24.3. For RotaTR, the APs are 31.1 and 30.9.

methods	MS downsample ratios					Params	mAP
	64	32	16	8	4		
Retinanet-O[19]						34M	60.3
	✓	✓	✓	✓		37M	66.3
	✓	✓	✓	✓	✓	38M	<b>67.1</b>
O2DETR[24]						38M	62.2
	✓	✓	✓	✓		41M	66.1
	✓	✓	✓	✓	✓	42M	<b>68.6</b>
						38M	62.9
Deform-DETR-O[54]	✓	✓	✓	✓		39M	67.2
	✓	✓	✓	✓	✓	40M	<b>68.6</b>
						38M	63.1
RotaTR	✓	✓	✓	✓		39M	72.0
	✓	✓	✓	✓	✓	40M	<b>72.3</b>
						38M	63.1

Table 7: Ablation on Multi-Level Features. The performance are reported on DOTA-v1.0 validation set.

**Effect of Range Restriction.** RotaTR restricts the range of the sampling locations. By default, the sampling points are restricted to be inside the reference anchor. While considering that the reference anchor may not be accurate, we introduce the parameter  $\alpha$  to control the sampling range. To verify the effect of the sampling range on the performance, we experiment on the offset range factor  $\alpha$ . The results are

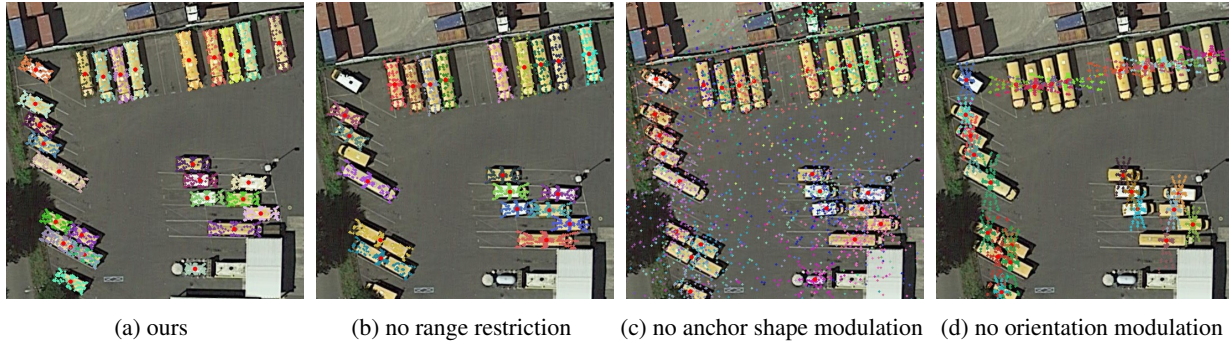


Figure 4: Sampled points of the deformable cross attention under different configurations. Red points represent the detected instance center, other colored points represent the sampled points for each instance. (a) Our default configuration. The sampled points are well aligned to the targets’ geometry. (b) Dropping the sampled points’ range restriction. Some points get out of the range of the objects. (c) Dropping the modulation from width and height. The sampled points span the whole image. (d) Dropping the modulation from the orientation. It represents the original Deformable Attention. The sampled points learn the width and height well, but the orientation is totally incorrect.

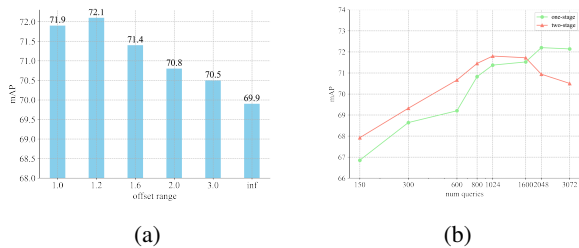


Figure 5: (a) Effect of the offset range restriction on the deformable sampling offsets. (b) Influence of the number of queries.

shown in Figure-5(a). It is seen that when no restriction, the performance only gets 69.2% mAP. The experiment results generally follow the pattern that the larger range, the lower performance. The effect of the range restriction can also be validated through the quality plot in Figure-4, in which the sampled points of the deformable attention are plot. It is seen that when no range restriction is applied, the sampled points are not strictly aligned with the target instance.

**Influence of Number of Queries.** The experiment for query number ablation is conducted for both one-stage and two-stage forms of RotaTR. The results are shown in Figure-5(b). Considering that the most number of instances per cropped patch is about 1,000, we think that setting the number of queries above 1,000 is appropriate. For the one-stage form, the increase of queries consistently leads to better performance. While for the two-stage form, the excess of queries will result in a performance drop. We argue that the essential influence is brought by the number of anchors. For the one-stage form, the number of anchors is simply defined by the randomly initialized queries. While the two-stage form makes use of every pixel of the feature maps as anchors and the number of queries only influences the top-K candidates’ selection of them. So, too many candidates may result in a large number of redundant proposals input to the decoder, which leads to the performance drop.

Method	Label Assign	AP50	AP75	AP50:95
One-Stage	O2O	70.67	47.48	44.47
	O2M	<b>72.01</b>	<b>49.02</b>	<b>45.11</b>
Two-Stage	O2O	<b>71.92</b>	<b>48.01</b>	<b>44.37</b>
	O2M	64.31	43.25	38.02

Table 8: Effect of label assignment. The results are reported on DOTA-v1.0 validation set. O2O is the short for the one to one matching and O2M is the short for one to many matching.

**Effect of Label Assignment.** In this experiment, we explore the effect of the label assignment of the alignment module. The label assignment method for the decoder part is kept unchanged. We only vary the label assignment for the first stage (feature alignment module and the encoder output) and the label assignment methods are chosen from the original one-to-one matching (O2O) scheme and the ATSS (O2M) scheme. The results are shown in Table-8. It is seen that the one-stage and two-stage form favors different assignment mechanisms. For the one-stage form, the O2M mechanism for the encoder output will result in better performance. For the two-stage form, only the O2O mechanism should be selected as the O2M will result in a huge performance decline (-7.61%AP). We argue that the two-stage form highly depends on good proposal generation, while the O2M label assignment will bring a large number of redundant candidates, thus deteriorating the decoding process.

## 5. Conclusion

This paper proposes RotaTR as an extension from the DETR to the oriented detection. We conduct experiments on several challenging oriented object detection benchmarks including the aerial object detection, ship detection and scene text detection. Experimental results show that our method has competitive accuracy to the state of the art.

## References

- [1] Nicolas Carion, Francisco Massa, Gabriel Synnaeve, Nicolas Usunier, Alexander Kirillov, and Sergey Zagoruyko. End-to-end object detection with transformers. In *European conference on computer vision*, pages 213–229. Springer, 2020.
- [2] Kai Chen, Jiaqi Wang, Jiangmiao Pang, Yuhang Cao, Yu Xiong, Xiaoxiao Li, Shuyang Sun, Wansen Feng, Ziwei Liu, Jiarui Xu, Zheng Zhang, Dazhi Cheng, Chenchen Zhu, Tianheng Cheng, Qijie Zhao, Buyu Li, Xin Lu, Rui Zhu, Yue Wu, Jifeng Dai, Jingdong Wang, Jianping Shi, Wanli Ouyang, Chen Change Loy, and Dahua Lin. MMDetection: Open mmlab detection toolbox and benchmark. *arXiv preprint arXiv:1906.07155*, 2019.
- [3] Yuntao Chen, Chenxia Han, Naiyan Wang, and Zhaoxiang Zhang. Revisiting feature alignment for one-stage object detection. *ArXiv*, abs/1908.01570, 2019.
- [4] Zhiming Chen, Kean Chen, Weiyao Lin, John See, Hui Yu, Yan Ke, and Cong Yang. Piou loss: Towards accurate oriented object detection in complex environments. In *European Conference on Computer Vision*, pages 195–211. Springer, 2020.
- [5] Bowen Cheng, Ishan Misra, Alexander G. Schwing, Alexander Kirillov, and Rohit Girdhar. Masked-attention mask transformer for universal image segmentation. *2022 IEEE/CVF Conference on Computer Vision and Pattern Recognition (CVPR)*, pages 1280–1289, 2022.
- [6] Bowen Cheng, Alexander G. Schwing, and Alexander Kirillov. Per-pixel classification is not all you need for semantic segmentation. In *NeurIPS*, 2021.
- [7] Jian Ding, Nan Xue, Yang Long, Gui-Song Xia, and Qikai Lu. Learning roi transformer for oriented object detection in aerial images. In *Proceedings of the IEEE/CVF Conference on Computer Vision and Pattern Recognition*, pages 2849–2858, 2019.
- [8] Kaiwen Duan, Song Bai, Lingxi Xie, Honggang Qi, Qingming Huang, and Qi Tian. Centernet: Keypoint triplets for object detection. In *Proceedings of the IEEE/CVF international conference on computer vision*, pages 6569–6578, 2019.
- [9] Jiaming Han, Jian Ding, Jie Li, and Gui-Song Xia. Align deep features for oriented object detection. *IEEE Transactions on Geoscience and Remote Sensing*, 60:1–11, 2021.
- [10] Kaiming He, Georgia Gkioxari, Piotr Dollár, and Ross B. Girshick. Mask r-cnn. *2017 IEEE International Conference on Computer Vision (ICCV)*, pages 2980–2988, 2017.
- [11] Wenhao He, Xu-Yao Zhang, Fei Yin, and Cheng-Lin Liu. Deep direct regression for multi-oriented scene text detection. In *Proceedings of the IEEE International Conference on Computer Vision (ICCV)*, Oct 2017.
- [12] Han Hu, Jiayuan Gu, Zheng Zhang, Jifeng Dai, and Yichen Wei. Relation networks for object detection. In *Proceedings of the IEEE conference on computer vision and pattern recognition*, pages 3588–3597, 2018.
- [13] Lichao Huang, Yi Yang, Yafeng Deng, and Yanan Yu. Densebox: Unifying landmark localization with end to end object detection. *ArXiv*, abs/1509.04874, 2015.
- [14] Sukjun Hwang, Miran Heo, Seoung Wug Oh, and Seon Joo Kim. Video instance segmentation using inter-frame communication transformers. *ArXiv*, abs/2106.03299, 2021.
- [15] Yingying Jiang, Xiangyu Zhu, Xiaobing Wang, Shuli Yang, Wei Li, Hua Wang, Pei Fu, and Zhenbo Luo. R2cnn: Rotational region cnn for orientation robust scene text detection. *arXiv preprint arXiv:1706.09579*, 2017.
- [16] Dimosthenis Karatzas, Lluís Gomez-Bigorda, Angelos Nicolaou, Suman Ghosh, Andrew Bagdanov, Masakazu Iwamura, Jiri Matas, Lukas Neumann, Vijay Ramaseshan Chandrasekhar, Shijian Lu, et al. Icdar 2015 competition on robust reading. In *2015 13th International Conference on Document Analysis and Recognition*, pages 1156–1160. IEEE, 2015.
- [17] Hei Law and Jia Deng. Cornernet: Detecting objects as paired keypoints. *International Journal of Computer Vision*, 128:642–656, 2019.
- [18] Minghui Liao, Zhen Zhu, Baoguang Shi, Gui-song Xia, and Xiang Bai. Rotation-sensitive regression for oriented scene text detection. In *Proceedings of the IEEE Conference on Computer Vision and Pattern Recognition (CVPR)*, June 2018.
- [19] T. Y. Lin, P. Goyal, R. Girshick, K. He, and P. Dollár. Focal loss for dense object detection. *IEEE Transactions on Pattern Analysis & Machine Intelligence*, PP(99):2999–3007, 2017.
- [20] Shilong Liu, Feng Li, Hao Zhang, Xiao Yang, Xianbiao Qi, Hang Su, Jun Zhu, and Lei Zhang. Dab-detr: Dynamic anchor boxes are better queries for detr. *arXiv preprint arXiv:2201.12329*, 2022.
- [21] Xiaolong Liu, Qimeng Wang, Yao Hu, Xu Tang, Shiwei Zhang, Song Bai, and Xiang Bai. End-to-end temporal action detection with transformer. *IEEE Transactions on Image Processing*, 31:5427–5441, 2022.
- [22] Zikun Liu, Liu Yuan, Lubin Weng, and Yiping Yang. A high resolution optical satellite image dataset for ship recognition and some new baselines. In *Proceedings of the International Conference on Pattern Recognition Applications and Methods*, volume 2, pages 324–331, 2017.
- [23] Jianqi Ma, Weiyuan Shao, Hao Ye, Li Wang, Hong Wang, Yingbin Zheng, and Xiangyang Xue. Arbitrary-oriented scene text detection via rotation proposals. *IEEE Transactions on Multimedia*, 20(11):3111–3122, 2018.
- [24] Teli Ma, Mingyuan Mao, Honghui Zheng, Peng Gao, Xi-aodi Wang, Shumin Han, Errui Ding, Baochang Zhang, and David Doermann. Oriented object detection with transformer. *arXiv preprint arXiv:2106.03146*, 2021.
- [25] Depu Meng, Xiaokang Chen, Zejia Fan, Gang Zeng, Houqiang Li, Yuhui Yuan, Lei Sun, and Jingdong Wang. Conditional detr for fast training convergence. In *Proceedings of the IEEE/CVF International Conference on Computer Vision*, pages 3651–3660, 2021.
- [26] Xingjia Pan, Yuqiang Ren, Kekai Sheng, Weiming Dong, Haolei Yuan, Xiaowei Guo, Chongyang Ma, and Changsheng Xu. Dynamic refinement network for oriented and densely packed object detection. In *Proceedings of the IEEE/CVF Conference on Computer Vision and Pattern Recognition*, pages 11207–11216, 2020.

- [27] W. Qian, Xue Yang, Silong Peng, Junchi Yan, and Xiujian Zhang. Rsdet++: Point-based modulated loss for more accurate rotated object detection. *IEEE Transactions on Circuits and Systems for Video Technology*, 32:7869–7879, 2022.
- [28] Joseph Redmon, Santosh Kumar Divvala, Ross B. Girshick, and Ali Farhadi. You only look once: Unified, real-time object detection. *2016 IEEE Conference on Computer Vision and Pattern Recognition (CVPR)*, pages 779–788, 2016.
- [29] Shaoqing Ren, Kaiming He, Ross Girshick, and Jian Sun. Faster r-cnn: Towards real-time object detection with region proposal networks. *Advances in neural information processing systems*, 28, 2015.
- [30] Baoguang Shi, Xiang Bai, and Serge Belongie. Detecting oriented text in natural images by linking segments. In *Proceedings of the IEEE conference on computer vision and pattern recognition*, pages 2550–2558, 2017.
- [31] Ding Shi, Yujie Zhong, Qiong Cao, Jing Zhang, Lin Ma, Jia Li, and Dacheng Tao. React: Temporal action detection with relational queries. In *ECCV*, 2022.
- [32] Xuepeng Shi, Shiguang Shan, Meina Kan, Shuzhe Wu, and Xilin Chen. Real-time rotation-invariant face detection with progressive calibration networks. In *Proceedings of the IEEE Conference on Computer Vision and Pattern Recognition*, pages 2295–2303, 2018.
- [33] Peize Sun, Yi Jiang, Enze Xie, Wenqi Shao, Zehuan Yuan, Changhu Wang, and Ping Luo. What makes for end-to-end object detection? In *International Conference on Machine Learning*, pages 9934–9944. PMLR, 2021.
- [34] Peize Sun, Rufeng Zhang, Yi Jiang, Tao Kong, Chenfeng Xu, Wei Zhan, Masayoshi Tomizuka, Lei Li, Zehuan Yuan, Changhu Wang, et al. Sparse r-cnn: End-to-end object detection with learnable proposals. In *Proceedings of the IEEE/CVF conference on computer vision and pattern recognition*, pages 14454–14463, 2021.
- [35] Zhi Tian, Chunhua Shen, Hao Chen, and Tong He. Fcos: Fully convolutional one-stage object detection. *2019 IEEE/CVF International Conference on Computer Vision (ICCV)*, pages 9626–9635, 2019.
- [36] Zhuotao Tian, Michelle Shu, Pengyuan Lyu, Ruiyu Li, Chao Zhou, Xiaoyong Shen, and Jiaya Jia. Learning shape-aware embedding for scene text detection. In *Proceedings of the IEEE/CVF Conference on Computer Vision and Pattern Recognition (CVPR)*, June 2019.
- [37] Jiaqi Wang, Kai Chen, Shuo Yang, Chen Change Loy, and Dahua Lin. Region proposal by guided anchoring. In *Proceedings of the IEEE/CVF Conference on Computer Vision and Pattern Recognition (CVPR)*, June 2019.
- [38] Jianfeng Wang, Lin Song, Zeming Li, Hongbin Sun, Jian Sun, and Nanning Zheng. End-to-end object detection with fully convolutional network. In *Proceedings of the IEEE/CVF conference on computer vision and pattern recognition*, pages 15849–15858, 2021.
- [39] Jinwang Wang, Wen Yang, Hengchao Li, Haijian Zhang, and Guisong Xia. Learning center probability map for detecting objects in aerial images. *IEEE Transactions on Geoscience and Remote Sensing*, 59:4307–4323, 2021.
- [40] Wenhai Wang, Enze Xie, Xiaoge Song, Yuhang Zang, Wenjia Wang, Tong Lu, Gang Yu, and Chunhua Shen. Efficient and accurate arbitrary-shaped text detection with pixel aggregation network. In *Proceedings of the IEEE/CVF International Conference on Computer Vision (ICCV)*, October 2019.
- [41] Yuqing Wang, Zhaoliang Xu, Xinlong Wang, Chunhua Shen, Baoshan Cheng, Hao Shen, and Huaxia Xia. End-to-end video instance segmentation with transformers. *2021 IEEE/CVF Conference on Computer Vision and Pattern Recognition (CVPR)*, pages 8737–8746, 2021.
- [42] Yingming Wang, Xiangyu Zhang, Tong Yang, and Jian Sun. Anchor detr: Query design for transformer-based detector. In *Proceedings of the AAAI conference on artificial intelligence*, volume 36, pages 2567–2575, 2022.
- [43] Junfeng Wu, Yi Jiang, Wenqing Zhang, Xiang Bai, and Song Bai. Seqformer: a frustratingly simple model for video instance segmentation. *ArXiv*, abs/2112.08275, 2021.
- [44] Gui-Song Xia, Xiang Bai, Jian Ding, Zhen Zhu, Serge Belongie, Jiebo Luo, Mihai Datcu, Marcello Pelillo, and Liangpei Zhang. Dota: A large-scale dataset for object detection in aerial images. In *Proceedings of the IEEE Conference on Computer Vision and Pattern Recognition*, pages 3974–3983, 2018.
- [45] Xingxing Xie, Gong Cheng, Jiabao Wang, Xiwen Yao, and Junwei Han. Oriented r-cnn for object detection. In *Proceedings of the IEEE/CVF International Conference on Computer Vision (ICCV)*, pages 3520–3529, October 2021.
- [46] Mingze Xu, Yuanjun Xiong, Hao Chen, Xinyu Li, Wei Xia, Zhuowen Tu, and Stefan O Soatto. Long short-term transformer for online action detection. *ArXiv*, abs/2107.03377, 2021.
- [47] Chuhui Xue, Shijian Lu, and Wei Zhang. Msr: Multi-scale shape regression for scene text detection. In *IJCAI*, 2019.
- [48] Xue Yang, Junchi Yan, Ziming Feng, and Tao He. R3det: Refined single-stage detector with feature refinement for rotating object. In *Proceedings of the AAAI conference on artificial intelligence*, volume 35, pages 3163–3171, 2021.
- [49] Xue Yang, Jirui Yang, Junchi Yan, Yue Zhang, Tengfei Zhang, Zhi Guo, Xian Sun, and Kun Fu. Srdet: Towards more robust detection for small, cluttered and rotated objects. *2019 IEEE/CVF International Conference on Computer Vision (ICCV)*, pages 8231–8240, 2019.
- [50] Cong Yao, Xiang Bai, and Wenyu Liu. A unified framework for multioriented text detection and recognition. *IEEE Transactions on Image Processing*, 23(11):4737–4749, 2014.
- [51] Cong Yao, Xiang Bai, Wenyu Liu, Yi Ma, and Zhuowen Tu. Detecting texts of arbitrary orientations in natural images. In *Proceedings of the IEEE Conference on Computer Vision and Pattern Recognition*, pages 1083–1090. IEEE, 2012.
- [52] Sixiao Zheng, Jiachen Lu, Hengshuang Zhao, Xiatian Zhu, Zekun Luo, Yabiao Wang, Yanwei Fu, Jianfeng Feng, Tao Xiang, Philip H. S. Torr, and Li Zhang. Rethinking semantic segmentation from a sequence-to-sequence perspective with transformers. *2021 IEEE/CVF Conference on Computer Vision and Pattern Recognition (CVPR)*, pages 6877–6886, 2021.
- [53] Xinyu Zhou, Cong Yao, He Wen, Yuzhi Wang, Shuchang Zhou, Weiran He, and Jiajun Liang. East: An efficient and

accurate scene text detector. In *Proceedings of the IEEE Conference on Computer Vision and Pattern Recognition (CVPR)*, July 2017.

- [54] Xizhou Zhu, Weijie Su, Lewei Lu, Bin Li, Xiaogang Wang, and Jifeng Dai. Deformable detr: Deformable transformers for end-to-end object detection. *arXiv preprint arXiv:2010.04159*, 2020.